
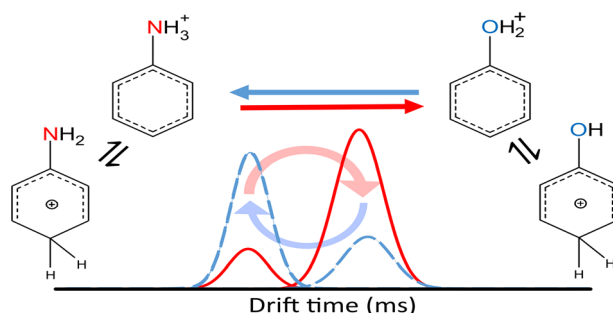


A Mechanistic Study of Protonated Aniline to Protonated Phenol Substitution Considering Tautomerization by Ion Mobility Mass Spectrometry and Tandem Mass Spectrometry

Christopher Kune,¹  Cédric Delvaux,¹ Jean R. N. Haler,^{1,2} Loïc Quinton,¹ Gauthier Eppe,¹ Edwin De Pauw,¹ Johann Far¹

¹MOLSYS, Mass Spectrometry Laboratory, University of Liège, Quartier Agora, Allée du Six Aout 11, B-4000, Liège, Belgium

²Department of Chemistry and Biochemistry, Florida International University, Miami, FL 33199, USA



Abstract. We report the use of ion mobility mass spectrometry (IMMS) and energy-resolved collisional activation to investigate gas-phase reactions of protonated aniline and protonated phenol. Protonated aniline prototropic tautomerization and nucleophilic substitution (SN1) to produce phenol with traces of water in the IMMS cell are reported. Tautomerization of protonated phenol and its ability to form protonated aniline in presence of ammonia in the gas phase are also observed.

These results are supported by energy landscapes obtained from computational chemistry. These structure modifications in the IMMS cell affected the measured collision cross section (CCS). A thorough understanding of the gas-phase reactions occurring in IMMS appears mandatory before using the experimental CCS as a robust descriptor which is stated by the recent literature.

Keywords: Ion mobility, Mass spectrometry, Tautomerism, Nucleophilic substitution, Aniline, Phenol, Gas-phase reaction, Computational chemistry

Received: 30 May 2019/Revised: 1 August 2019/Accepted: 11 August 2019/Published Online: 13 September 2019

Introduction

A collision cross section (CCS) is usually experimentally obtained from ion mobility spectrometry (IMS). Ion mobility coupled to mass spectrometry (IMMS) provides both CCS values and mass spectra (m/z) in a single experiment. Analytical chemistry applications recently found interest in the use of IMMS to increase peak capacity, thus resulting not only in a better signal-to-noise ratio in mass spectra [1, 2], but also in the use of the CCS as a new ion descriptor for the identification of

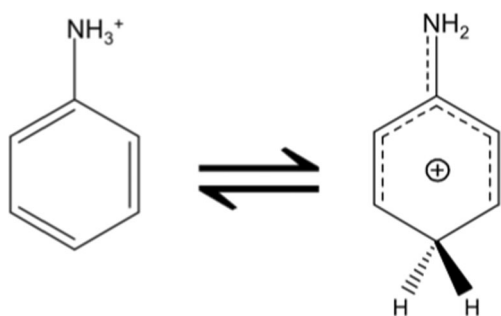
compounds such as pesticides or metabolites [3–6]. To play that role, IMMS must provide a unique and reproducible CCS value. Nonetheless, several authors already suggested that the observed arrival time distribution (ATD) or equivalent quantities (e.g., ramping voltage profile) leading to the CCS could be affected by ion diffusion and gas-phase reactions occurring in-source or during the separation of ions in the mobility devices [7–10]. Understanding gas-phase reactions and their effects on ion mobility profiles is then pivotal to enhance confidence in the CCS values as a unique ion descriptor. Most of the gas-phase reactions reported in literature are tautomerism reactions. Among them, the most common form of tautomerism is prototropy, which refers to the relocation of proton(s) within the same organic compound [11]. Prototropic tautomers, also known as “protomers”, are a set of ions sharing the same empirical formula, electron parity, and total charge but characterized by different

Electronic supplementary material The online version of this article (<https://doi.org/10.1007/s13361-019-02321-4>) contains supplementary material, which is available to authorized users.

Correspondence to: Christopher Kune; e-mail: c.kune@uliege.be

protonation sites [12]. The most published studies of prototropic tautomers concern protonated aromatic compounds, especially aniline and phenol [13]. Most of these experimental and theoretical studies were carried out in the gas phase with notable disagreements concerning the result interpretation even in recent papers [13–19]. In the case of aniline, the major controversial issue was the determination of the preferred protonation site in the gas phase. Experimental evidence obtained by Fourier-transform ion cyclotron resonance mass spectrometry (FT-ICR-MS) and deuterium labeling of aniline suggested a preferential protonation at the amino group [15], while ion mobility mass spectrometry (IMMS) showed the detection of two ion mobility distributions with relative intensities of 90% and 10% [14, 20]. These two distributions were attributed to C_{para} -protonated (protonation at the para-position of the aromatic ring) and N-protonated aniline (protonation at the nitrogen of the amino group) tautomers, respectively (see Scheme 1) [15, 18]. Ab initio calculation studies were also used to elucidate this issue but the results were very sensitive to the choice of the computational method [16, 17]. The theoretical approaches were based on density functional theory (DFT) using the highest calculation-level methods available. The results suggest that C_{para} -protonated aniline is favored by only 0.5–0.7 kcal/mol (estimated computational error is around 1 kcal/mol) compared N-protonated aniline. Consequently, the protonation of aniline should provide both species in roughly equal amounts instead of the experimental 9:1 ratio obtained from IMMS experiments. It was therefore stated that the N-protonated isomer was kinetically preferred.

Similar experimental investigations of the protonation sites of phenol in the gas-phase suggested that the protonation occurs on the aromatic ring [21, 22]. However, the protonation could also take place on the hydroxyl group (O-protonated phenol). Theoretical calculations suggested that the carbon in para-position is the favored protonation site of the phenol (C_{para} -protonated phenol) [23]. The ratio of tautomers observed in IMMS was affected by tautomerization in the gas phase and was strongly dependent on the experimental settings [19, 24], affecting the experimental CCS determination. Moreover, the fragmentations of aniline and phenol lead both to the formation of phenyl cations, a highly reactive intermediate towards the addition of N- or O-containing compounds [25], which could also affect the experimental CCS determination.



N-protonated aniline C_{para} -protonated aniline
Scheme 1. N-protonated aniline and C_{para} -protonated aniline

In this study, we propose the use of ion mobility and energy-resolved ion activations to improve our understanding of the gas-phase reactions affecting the experimental arrival time distributions of aniline and phenol. We also report the detection of protonated phenol when a solution of pure aniline is infused in a TWIMS (Synapt G2 HDMS Waters, UK). We point out that IMMS is well-suited for experimentally identifying and investigating gas-phase reactions (i.e., tautomerization and nucleophilic substitution). The evolution of relative intensities corresponding to the signals of the ionic species as a function of the activation energy suggests mechanisms of reaction supported by computational chemistry.

Experimental

Samples

Aniline, phenol, formic acid, and tetraalkylammonium bromides were purchased from Sigma-Aldrich (Belgium). UPLC MS grade methanol and acetonitrile were purchased from Biosolve (France). Ultrapure water was freshly prepared from a milliQ Millipore system (Millipore, Molsheim, France). Aniline and phenol were respectively dissolved in pure acetonitrile and pure water, respectively, to obtain stock solutions of 0.1 M. Tetraethylammonium bromide, tetrapropylammonium bromide, tetrabutylammonium bromide, and tetrapentylammonium bromide were separately dissolved in ultrapure water to prepare stock solutions of 1 mM. Tetrahexylammonium bromide, tetraheptylammonium bromide, and tetraoctylammonium bromide were dissolved in methanol to obtain stock solutions of 1 mM. A total of 10 μM of aniline in acetonitrile/water (50/50, v/v) solution and 100 μM of phenol in acetonitrile/water (50/50, v/v) solution were infused in the ESI-IMMS Synapt G2 HDMS spectrometer. One percent of formic acid was added to these infusion solutions to promote the protonation. A mixture of 1 μM of each tetraalkylammonium in acetonitrile/water (50/50, v/v) solution was infused for calibrating the CCS and the traveling wave IMS (TWIMS) diffusion [7]. N50 grade (99.999%) carbon dioxide compressed gas including ≤ 50 ppm of water content, and Alphagas2 grade (≤ 0.5 ppm of water content) of helium, argon, and nitrogen was purchased from Air Liquide (Belgium). Alphagas2 grade specifies water and contaminant volatile contents below 0.5 ppm per mole and a global purity of more than 99.9999%. Ammonia gas was purchased from Air Liquide (Belgium) at grade 5.0 (i.e., 99.999% including ≤ 3 ppm of water content). Ion mobility drift gas spiked with ammonia using a micro-valve and a stainless steel tee connector to reach approximately 1–2% of the drift gas flow rate.

Ion Mobility Mass Spectrometry and Energy-Resolved Collision-Induced Dissociation Experiments

Tandem mass spectra and ATD presented in this paper were all acquired using a Waters Synapt G2 HDMS (UK). Pressures were measured using independent capacitance gauges

(Oerlikon Q5 Leybold Vacuum, CERAVAC CTR 90) linked to a vacuum controller (Vacom, MVC-UVH Multichannel Vacuum Controller). The ion mobility cell of the Synapt G2 HDMS is a traveling wave ion mobility cell (TWIMS cell) [26]. The source voltage was set to +3 kV. The sampling cone and extraction cone voltages were set to 25 V and 4 V, respectively. The source temperature was 100 °C. The drift gas was carbon dioxide (CO₂) at an apparent pressure of 2.8 mbar. The mass-to-charge ratio (m/z) range was set from 50 to 1200. CO₂ was used in most measurements reported in this work to enhance the separation of tautomers based on their interactions with the polarizable drift gas [27, 28]. N₂ was also tested as drift gas (see discussion for details). The IMMS separation is therefore enhanced if, as expected, dipole moments of the tautomers are noticeably different. The experiments involving ammonia drift gas were performed using a stainless steel tee and a precision valve. Note that this experiment could probably damage the N₂ mass flow controller of the ion mobility spectrometer. The TRAP and the TRANSFER collisional-induced dissociation (CID) collision cells, which are placed before and after the IMS cell respectively (see Figure S1 in supplemental information), were filled with 5.8×10^{-1} mbar of Ar. Velocity and height of the traveling waves were respectively fixed at 1000 m s⁻¹ and 40 V. No experimental CCS values are reported from TWIMS data due to the lack of CCS calibrant ions in CO₂. IMS peak deconvolutions were assisted using the TWIMS diffusion calibration strategy previously published [7]. Data were processed using MassLynx V4.1 and peak deconvolutions were achieved using Peakfit v4.11 (Peakfit settings were baseline = linear D2, peak type = spectroscopy and Gauss Amp, peak diffusion references were tetraalkylammonium). MSMS and breaking curves experiments used LMQuad = 15. The trapped ion mobility spectrometer (TIMS, timsTOF HD from Bruker, Germany) was used to obtain high-resolution ion mobility separation of aniline protomers. The TIMS cell was operated with N₂ as drift gas. ESI and end plate voltages were respectively set to 4 kV and -500 V. Dry gas was 3 L min⁻¹ at 200 °C. The TIMS ramp duration was 50 ms. The 1/K₀ start and end ramp values were fixed to 0.45 and 0.55 V s cm⁻², respectively. Quadrupole windows selection was set to $m/z = 94.06 \pm 0.5$. The m/z range was set from 50 to 1500. The ^{TIMS}CCS_{N₂} values reported in Figure 2 were obtained from a CCS calibration using the Agilent Tune Mix (Part No: G1969-85000). TIMS data were processed using Data Analysis v.5.1.

Computational Chemistry

Five protonation sites were investigated for phenol and aniline: the protonation of the heteroatom (oxygen for phenol and nitrogen for aniline, later referred as O-protonated and N-protonated, respectively), the protonation of the aromatic ring in ipso- (C_{ipso}-protonated), ortho- (C_{ortho}-protonated), meta- (C_{meta}-protonated), and in para- (C_{para}-protonated) positions. ChemDraw software (ChemOffice 2013 suite, Perkin Elmer) was used to design the 2D chemical structures. Stable

structures and zero-point energies of the protonated aniline and phenol tautomers, of the phenyl cations, were obtained from density functional theory (DFT) optimizations using Gaussian09d [29]. The global minimum structures were validated by verifying the absence of imaginary values of vibrational frequencies. The transition states of the tautomerization and of the nucleophilic substitution structures were obtained using the synchronous transit-guided quasi-Newton (STQN) method implemented in Gaussian09d software [30]. The structures of the optimized transition states were confirmed by the presence of only one imaginary frequency per structure. All atoms were described using the CAM-B3LYP functional [31] and the 6-31g++(d,p) basis set. IMoS v1.06e software was used to calculate the theoretical CCS in N₂ (polarization volume = 1.7 Å³, gas radius = 1.50 Å) and CO₂ (polarization volume = 3.0 Å³, gas radius = 1.98 Å) using the trajectory method (TM) at 300 K [32–34]. IMoS parameters were N_{gas} = 50,000, 92% Maxwell remission velocity and 92% Maxwell distributed. TM was preferred for CCS calculations instead of the projection approximation (PA) or exact hard sphere scattering (EHSS) algorithms to take into account ion-induced dipole interactions between the CO₂ drift gas molecules and the partial charges from the ions of interest through Lennard-Jones potential parameters [35–37]. ParsIMoS was used to convert the output files from Gaussian to the input files for IMoS [38].

Results and Discussion

Protonated Aniline to Protonated Phenol Conversion

The arrival time distribution (ATD) obtained from the traveling wave instrument of protonated aniline ([C₆H₈N]⁺, m/z 94.07) is reported in Figure 1A.

This ATD, as well as all the others met in this article, was deconvoluted using the previously published diffusion calibration method [7]. Briefly, the peaks' FWHM of the species of interest was accurately determined considering the ion diffusion in IMMS cell using tetraalkylammonium as diffusion calibrants. These FWHM values were then used to fix the parameters of ATD deconvolution assuming Gaussian peak shapes. The aniline signal deconvolution led to three distributions. Peaks at 5.15 ms and 6.01 ms were identified as the C_{para}-protonated aniline and N-protonated aniline, respectively, both in agreement with literature [14, 15, 18, 19]. In this work, the use of ion mobility mass spectrometry (Synapt G2 HDMS) with a higher resolving power than the Synapt G1 and CO₂ as drift gas provided slightly better tautomer separation than the previous studies. In Figure 1A, an intermediate distribution at 5.41 ms was added to better fit the experimental data. It could be explained by the presence of other tautomers (ortho, meta, or ipso position, see Figure 5A) or gas-phase tautomerization of aniline during IMS analyses. This was confirmed by the detection of a specific fragment from protonated aniline (m/z 64.93) after precursor selection and CID activation between the mobility peaks of C_{para}-protonated and N-protonated aniline using

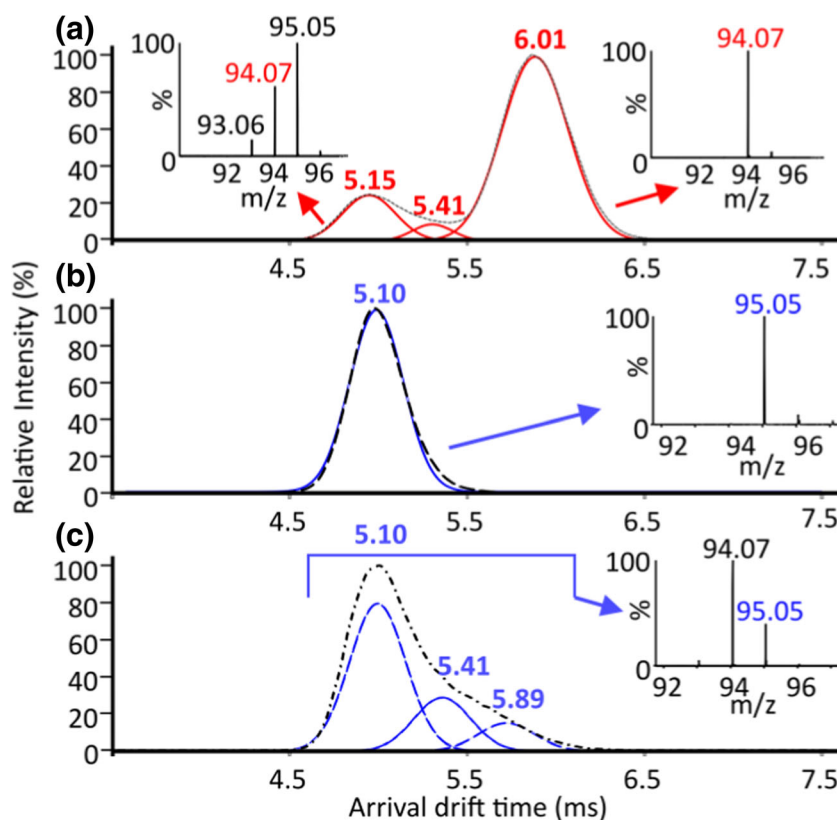


Figure 1. (a) ATD of protonated aniline in CO_2 from pure aniline dissolved in acetonitrile/water (50/50, v/v). (b) ATD of protonated phenol in CO_2 from pure phenol dissolved in acetonitrile/water (50/50, v/v). (c) ATD of protonated phenol formed during IMMS analysis from pure aniline solution. In red: extracted ion ATD of protonated aniline (m/z 94.07). In blue: extracted ion ATD of protonated phenol (m/z 95.07)

the Synapt G2 instrument (see Figure S2 in supplemental information). The intermediate distribution of aniline (detected by this specific fragment) was supported by using a higher resolution IMMS instrument (trapped ion mobility spectrometer with an experimental resolving power up to 150) as reported in Figure 2. The specific fragment at m/z 64.93 was also detected between the mobility peaks of C_{para} -protonated and N-protonated aniline. These data provide new evidence that the presence of other tautomers or gas-phase tautomerization led to an intermediate distribution having an experimental CCS of 114 \AA^2 . This value is compatible with the computed CCS of ortho (111 \AA^2), while meta- and ipso-proton positions were 110 and 109 \AA^2 respectively. Note that the ortho-protonated aniline is also more stable than the meta- or ipso-protonated aniline according to theoretical calculation (Figure 5). Moreover, these calculations also suggested that C_{ortho} -protonated aniline is a probable reaction intermediate of the C_{para} -protonated aniline and N-protonated aniline conversion.

Two other mass peaks were also detected in the ATD (Synapt G2 HDMS) of protonated aniline at 5.15 ms (Figure 1A). These ions were attributed to a specific fragment of C_{para} -protonated aniline ($\text{C}_6\text{H}_7\text{N}^+$, m/z 93.06) and to protonated phenol ions ($\text{C}_6\text{H}_7\text{O}^+$, m/z 95.05). The m/z 93.06 fragment ion was already reported in literature and is characteristic of a hydrogen loss from C_{para} -protonated aniline [18]. Interestingly, the m/z 93.06 fragment from aniline was sparsely detected

between the ATD of C_{para} -protonated aniline and N-protonated aniline, supporting the isomerization (actually tautomerization) of aniline during the IMS separation or the presence of another protonated aniline tautomer. Indeed, the detection of a specific fragment of C_{para} -protonated aniline in the ATD corresponding to N-protonated aniline requires the presence of the C_{para} -protonated aniline ion at this specific ATD. The detection of protonated phenol in MS spectra while infusing a standard solution of pure aniline strongly suggests a gas-phase substitution of the amino group from the protonated aniline (leaving group as NH_3) by a hydroxyl group inside the ion mobility mass spectrometer.

To confirm this gas-phase substitution reaction hypothesis, ATD of $100 \mu\text{M}$ of pure phenol solution infusion (Figure 1B) was compared with the ATD of the protonated phenol formed during the infusion of the pure aniline solutions (Figure 1C). The infused pure phenol solution led to only one ion distribution at 5.10 ms (see Figure 1B), which was assigned to C_{para} -protonated phenol based on previously published results [23]. Contrary to the phenol infusion, the deconvolution of ATD of protonated phenol from aniline infusion led to at least three ATDs (see Figure 1C). The first distribution has a similar average drift time (5.10 ms) as the ATD of the C_{para} -protonated phenol obtained during the infusion of the pure phenol solution (Figure 1B, C). The two other distributions at 5.41 ms and 5.89 ms could be attributed, respectively, to other protonated

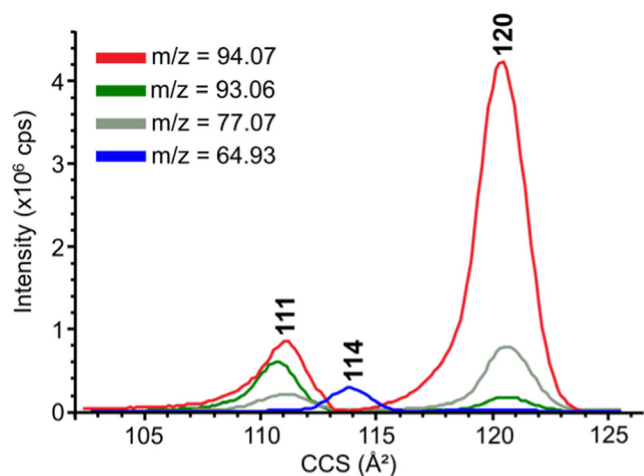


Figure 2. High-resolution ion mobility mass spectrometry (timsTOF) of protonated aniline (red line, m/z 94.07) and its fragments formed after IMS separation (m/z 93.06) in green (H loss), m/z 77.07 (phenyl cation) in gray, and m/z 64.93 (NHCH_2 loss) in blue line. Fragments were detected with the elution voltage of the precursor ions (CID performed after IMS separation). Protonated aniline was isolated by the quadrupole mass filter (m/z 94.06 ± 0.5). Experimental CCS_{N_2} values of the two distributions of protonated aniline (red line) are $111 \pm 2 \text{ \AA}^2$ and $120 \pm 2 \text{ \AA}^2$ which are in good agreement with the theoretical $^{\text{TM}}\text{CCS}_{\text{N}_2}$ of, respectively, C_{para} -protonated aniline (111 \AA^2) and N-protonated aniline (119 \AA^2). Effective resolving power = 50 (CCS/FWHM)

phenol tautomers such as O-protonated phenol (which is the second most stable tautomer according to computational chemistry) and protonated phenol formed from protonated aniline (nucleophilic substitution) during IMS separation (see Figure 1A and C), or a combination of both hypotheses.

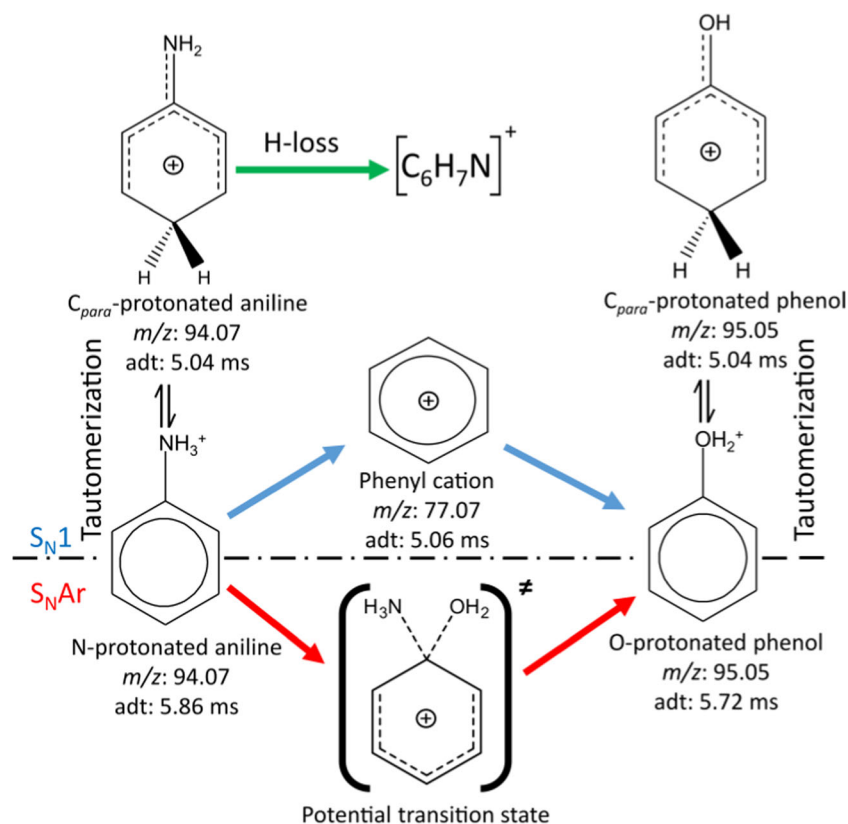
The protonated aniline to protonated phenol substitution hypothesis was confronted with experimental results, especially from energy-resolved collision-induced dissociation performed after the ion mobility separation using the Synapt G2 HDMS instrument. This nucleophilic substitution requires the intervention of a hydroxyl donor such as water. The reaction can be explained by two mechanisms of nucleophilic substitution involving either N-protonated aniline or O-protonated phenol as reported in Scheme 2. The first mechanism ($\text{S}_{\text{N}}1$) relies on a two-step nucleophilic substitution reaction. First, a stable phenyl cation (C_6H_5^+ , m/z 77.07) is formed by neutral loss of ammonia from protonated aniline. Then, a hydroxyl donor (e.g., a water molecule or water cluster present in the gas phase) bonds to the phenyl cation to form the protonated phenol ion as already suggested by the works of Ranasinghe, Glish, and Begala [25, 39]. Alternatively, the second mechanism ($\text{S}_{\text{N}}\text{Ar}$) is a one-step reaction involving protonated aniline and water. In this mechanism, the C–N bond of aniline is simultaneously broken while the C–OH bond of phenol is being formed. Both mechanisms are in agreement with the formation of O-protonated phenol as experimentally suggested by the presence of different distributions of protonated phenol in the ATD from a pure infused aniline solution (Figure 1C). It

is important to notice that the $\text{S}_{\text{N}}\text{Ar}$ mechanism requires an excess of water, which can be reasonably discarded as a major constituent of the gas phase. Tautomerism and nucleophilic substitution are thus two competitive reactions for N-protonated aniline. The left part of Scheme 2 shows the tautomerization and C_{para} -protonated aniline formation, explaining the presence of the H-loss fragment (m/z 93.06) detected in the ATD of C_{para} - and N-protonated aniline. The center and right parts of Scheme 2 show the nucleophilic substitutions ($\text{S}_{\text{N}}1$ or $\text{S}_{\text{N}}\text{Ar}$) and protonated phenol formation, explaining the detection of protonated phenol from aniline infusion.

The presence of (at least) a water molecule is mandatory for the nucleophilic substitution ($\text{S}_{\text{N}}1$ or $\text{S}_{\text{N}}\text{Ar}$). The water could be supplied by the feed gases, i.e., the ion source, and the traveling wave ion mobility cell. To investigate the reaction mechanisms occurring during the ion mobility separation, pure solutions of aniline and phenol were separately infused into the Synapt G2 HDMS. The presence of water molecules in the instrument after ion desolvation can therefore be confirmed by comparing the pre-IMS activation and the post-IMS activation by collisional induced dissociation (CID). The Synapt G2 HDMS allows gas-phase activation of ions by collisions before (in the so-called TRAP cell) and after (in the so-called TRANSFER cell) the IMS cell. If traces of water are present in the IMS cell, product ions produced in the TRAP cell would be in contact with these water molecules in the IMS cell contrary to the ions formed in the TRANSFER cell. The positions of these two CID cells are provided in the schematic representation of the Synapt G2 HDMS (see Figure S1 in supplemental information).

Relative ion intensities of protonated aniline, phenol, and phenyl cation as a function of the CID energy (i.e., acceleration voltage in volts) and the selected cell for activation are reported in Figure 3. Protonated aniline (m/z 94.07), protonated phenol (m/z 95.05), and phenyl cation (C_6H_5^+ , m/z 77.07) are reported in red, blue, and gray, respectively.

The relative intensities of the most abundant ions from an infused $10 \mu\text{M}$ pure aniline solution as a function of the CID in the TRANSFER cell are reported in Figure 3A. The quadrupole of the Synapt G2 HDMS was used to isolate the ions with m/z of 94.05 (protonated aniline) before the CID activation. As expected, the relative intensity of protonated aniline decreased while the intensity of phenyl cation rose with the increase of CID voltage. This supports the hypothesis that the CID activation of protonated aniline ions in the TRANSFER cell leads to the formation of phenyl cations by ammonia (NH_3) loss. The inflection point of the curve (which corresponds to 50% survival yield of ions that can be converted, also called V_{50}) is 15 V for protonated aniline. The presence of protonated phenol (m/z 95.06, relative intensity of 20% at 0 V) after the quadrupole selection of the m/z 94.05 precursor ion (protonated aniline) is due to the poor selection of the quadrupole of the Synapt G2 HDMS. The relative intensity of phenyl cation reached approximately 60% when only 45% of protonated aniline was converted. This supports that protonated phenol could also



Scheme 2. The S_N1 (blue arrows) and S_NAr (red arrows) mechanisms of nucleophilic substitution on protonated aniline. Competitive reactions are also reported in this scheme (the tautomerization with black double arrows and specific fragmentation of C_{para} -aniline in green arrow). “adt” is the acronym of average arrival drift time.

form phenyl cation through the loss of water after CID activation in the TRANSFER cell. The phenyl cation formation from protonated phenol is confirmed by the relative intensities of the most abundant ions from an infused 10 μ M pure phenol solution as a function of the CID voltage (Figure 3B). Indeed, the relative intensity of protonated phenol decreased while the relative intensity of phenyl cation increased with the increase of the TRANSFER CID voltage. The V_{50} value for protonated phenol is 13 V suggesting that the C–O bond of protonated phenol is weaker than the C–N bond of protonated aniline. Interestingly, both protonated aniline and protonated phenol ions could never be totally converted to phenyl cations by CID activation (Figure 3A, B). This further underlines the fact that the tautomerization could be induced by CID activation, leading to the formation of prototropic tautomers which cannot form phenyl cations by fragmentation as suggested in Scheme 2. The randomization of tautomer population (of both protonated aniline and protonated phenol) is thus assumed to be faster than the fragmentation by CID.

The formation of phenyl cation from protonated aniline by CID activation in the TRANSFER cell is observed for both C_{para} -protonated aniline and N-protonated aniline. The relative intensities of the most abundant ions at 5.15 ms (corresponding to the average arrival drift time of C_{para} -protonated aniline) and 6.01 ms (corresponding to the average arrival drift time of N-protonated aniline) as a function of the CID voltage in the

TRANSFER cell are respectively reported in Figure 3C, D. The quadrupole of Synapt G2 HDMS was again used to isolate the m/z 94.05 precursor ion (i.e., protonated aniline) before CID activation. The increase of phenyl cation intensity with the CID voltage revealed that both prototropic tautomers of aniline can lose NH_3 by CID activation. The presence of phenol (60% at 0 V for Figure 3C and 2% at 0 V for Figure 3D) was again due to the poor selection of the Synapt G2 quadrupole. Nevertheless, the relative intensity of phenyl cation at high CID voltages (above 20 V) was greater than the initial relative intensity of protonated phenol (in both figures), confirming that both tautomers of protonated aniline provide a phenyl cation during the fragmentation. This also supports the randomization of tautomers during CID process. The measured V_{50} value is 15 V regardless of the considered tautomer ion. These similarities between V_{50} values imply that the required fragmentation energy to form the phenyl cation does not depend on the protonation site. However, these similar fragmentation energies also indicate that the same bond was involved during the dissociation. This strongly suggests that a C_{para} -protonated aniline must be converted into an N-protonated aniline by tautomerization before the neutral loss of NH_3 to produce a phenyl cation, as depicted in Scheme 2.

Protonated aniline was converted into protonated phenol when the CID activation occurred before the IMS separation. Indeed, the relative intensity of protonated aniline decreased while the relative intensity of protonated phenol increased with

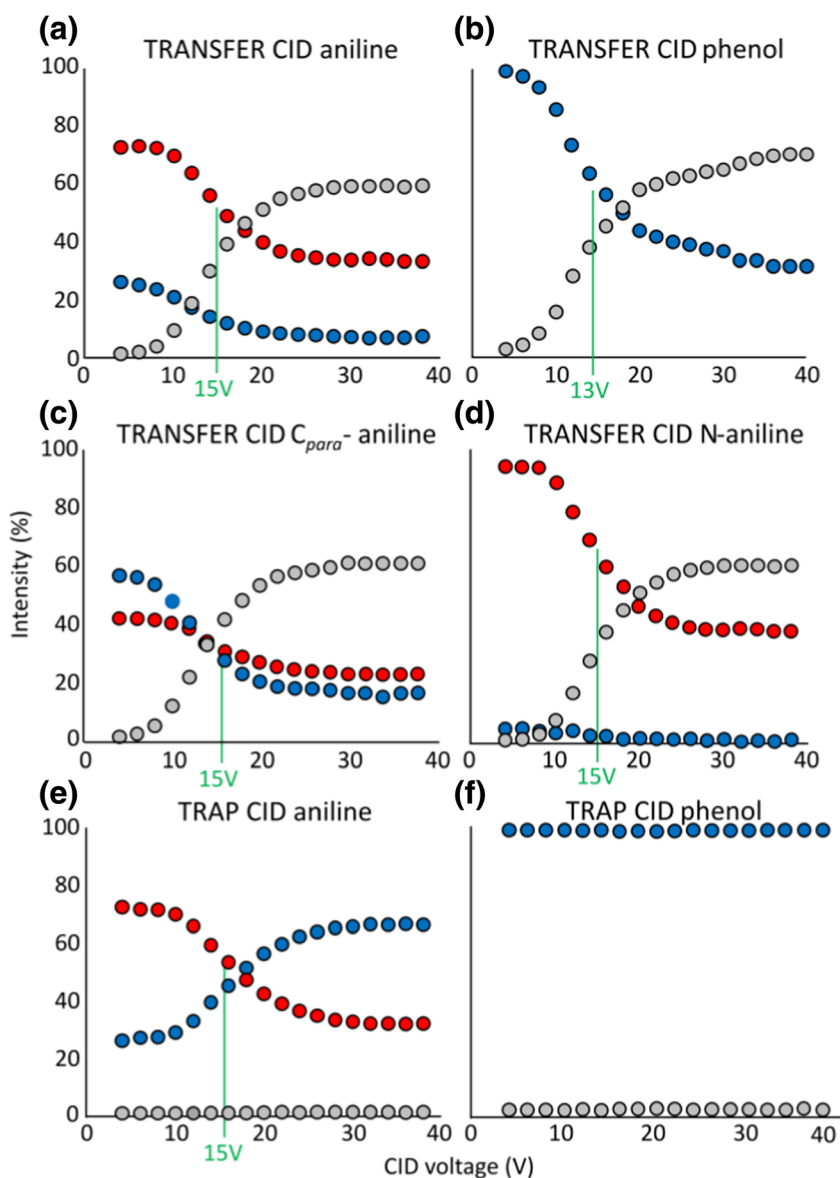


Figure 3. Relative intensity of protonated aniline (red dots), protonated phenol (blue dots), and phenyl cation (gray dots) as a function of the precursor ion and the CID voltage (in the TRAP and TRANSFER CID cells). (a) Product ions from protonated aniline (C_{para} -protonated aniline and N-protonated aniline) formed in the TRANSFER cell. (b) Product ions from total protonated phenol formed in the TRANSFER cell. (c) Product ions from C_{para} -protonated aniline (extracted at 5.15 ms) formed in the TRANSFER cell. (d) Product ions from N-protonated aniline (extracted at 6.01 ms) formed in the TRANSFER cell. (e) Product ions from protonated aniline (C_{para} -protonated aniline and N-protonated aniline) formed in the TRAP cell. (f) Product ions from protonated phenol form in the TRAP cell

the TRAP CID voltage (Figure 3E). These observations strongly suggest that the nucleophilic substitution occurs during the IMS separation, revealing the presence of water inside the IMS cell. The same V_{50} values of the protonated aniline (15 V) are obtained from CID performed in both the TRAP and the TRANSFER CID cells. This similarity suggests that the required energies (activation energy barriers) to form the phenyl cation (by CID fragmentation) or the protonated phenol (by nucleophilic substitution) are very close. We might conclude that the CID activation always leads to the formation of the phenyl cation, regardless of the activation cell (i.e., in TRAP or TRANSFER cells). Then, this phenyl cation easily produces

protonated phenols by the addition of a water molecule (or water cluster) present in the IMS cell. In our case, if the phenyl cation was produced before the IMS cell (TRAP CID cell), it would interact with a water molecule from the drift gas impurities and convert back to a protonated phenol ion. Alternatively, the lower apparent pressure in the TRANSFER cell (5.8×10^{-1} mbar) compared with the IMS cell (2.8 mbar) reasonably reduces the probability to encounter water, therefore limiting the formation of protonated phenol. This mechanism pathway is further supported by the high reactivity of the phenyl cation, as shown by its almost complete conversion to protonated phenol when the phenyl cation was intentionally produced by CID before the

IMS cell (Figure 3E). This two-step mechanism, i.e., neutral loss of NH_3 and the water addition, fits with the $\text{S}_{\text{N}}1$ reaction mechanism where the phenyl cation acts as an intermediate product ion during the reaction pathway (Scheme 2). On the other hand, we assume that the $\text{S}_{\text{N}}\text{Ar}$ mechanism would lead to the observation of different V_{50} values in TRAP and TRANSFER cells because the fragmentation and $\text{S}_{\text{N}}\text{Ar}$ nucleophilic substitution are two independent reactions. Moreover, The $\text{S}_{\text{N}}\text{Ar}$ nucleophilic substitution is a competitive reaction between NH_3 and H_2O additions, which should require higher water content concentration to favor the formation of protonated phenol instead of protonated aniline (contrary to $\text{S}_{\text{N}}1$ mechanism).

A similar result was observed for the infusion of a pure phenol solution. The intensity of protonated phenol does not decrease when the CID activation occurs in the TRAP cell (Figure 3F). This result can still be explained by an $\text{S}_{\text{N}}1$ reaction, as observed for protonated aniline. The protonated phenol is converted into a phenyl cation when the CID energy activation reaches the fragmentation energy. Then, the phenyl cation interacts with a water molecule present in the IMS cell to form the protonated phenol. The protonated phenol is then converted to a new protonated phenol through a phenyl cation intermediate, leading to the detection of a stable amount of protonated phenol, independent of the applied TRAP CID energy.

We also report that the use of nitrogen (alphagas2 grade) containing a lower amount of water than carbon dioxide N50 (as claimed by the manufacturer specifications) provided roughly similar IMS and CID results (data not shown). This difference in water content affects the relative intensity of detected protonated phenol from 2% in N_2 to 15% in CO_2 .

This result suggests that aniline infusion could be used to estimate the amount of moisture present in the gas phase.

Protonated Phenol to Protonated Aniline Conversion

To confirm the $\text{S}_{\text{N}}1$ mechanism hypothesis, the conversion of protonated phenol to protonated aniline in the presence of ammonia (NH_3) was investigated. As expected, the infusion of a pure phenol solution in the absence of NH_3 in the gas phase does not allow the detection of protonated aniline in the mass spectrum (Figure 4A). NH_3 was provided inside the Synapt G2 HDMS using two different approaches. First, 100 μM glutamine was co-infused with phenol solution to act as a neutral NH_3 donor (obtained by CID activation with a TRAP CID voltage of 10 V) [40]. The presence of NH_3 in gas phase led to the formation of protonated aniline from protonated phenol (Figure 4B). The second approach consisted of the direct introduction of NH_3 in the CO_2 drift gas and CID activation before IMS cell ((TRAP CID voltage of 10 V). In this experiment, protonated aniline ions were also observed in the mass spectrum of pure phenol solution (Figure 4C). These two results support the formation of protonated aniline from protonated phenol by an $\text{S}_{\text{N}}1$ mechanism involving the phenyl cation as reaction intermediate.

Investigation of Protonated Aniline and Protonated Phenol Interconversion Using Computational Chemistry

All possible prototropic tautomers were computed using DFT. The transition states were determined using the synchronous

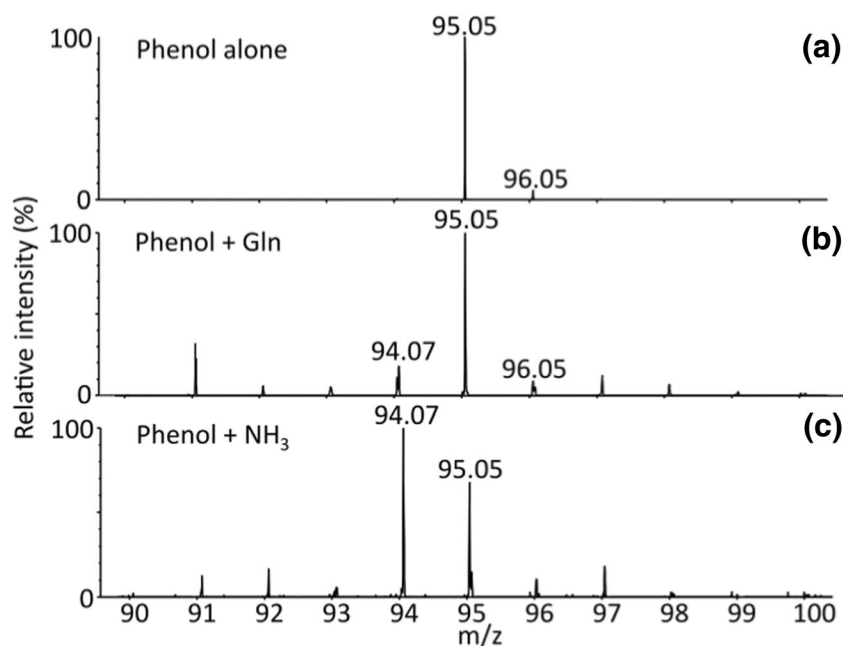


Figure 4. (a) Mass spectrum of pure phenol dissolved in acetonitrile/water (50/50, v/v). (b) Mass spectrum of a mixture of glutamine (ammonia donor) and phenol solution using a CID voltage of 10 V applied in the TRAP cell. (c) Mass spectrum of pure phenol dissolved in acetonitrile/water (50/50, v/v) injected inside the IMS cell filled with CO_2 spiked with NH_3 as drift gas and CID activation in the TRAP cell (10V). The m/z 94.07 and 95.05 correspond to protonated aniline and protonated phenol, respectively

transit-guided quasi-Newton method for assessing the activation energies. These resulting values allowed building the potential energy diagram provided in Figure 5. The reported energies for the mechanism pathways in Figure 5A, B are Gibbs free energy variations (ΔG° in kJ mol^{-1}) relative to the C_{para} -protonated aniline or C_{para} -protonated phenol, respectively. Stable structure energies are represented with black marks and transition state energies are represented with red spots. The reported ΔG° values of the phenyl cation were corrected by the addition of the G° values of the fragment lost (NH_3 for protonated aniline tautomerization mechanism and H_2O for protonated phenol tautomerization mechanism). These corrected ΔG° values considered all steps of the mechanism

with identical elemental composition to allow the direct comparison between all reported ΔG° values. The C_{para} -protonated and N-protonated prototropic tautomers of aniline shared similar ΔG° values (difference of 5 kJ mol^{-1}), which is in excellent agreement with the experimental detection of the two tautomers during IMMS experiments (Figure 1A). In the case of phenol, C_{para} -protonated phenol was by far the most stable tautomer as experimentally confirmed by the presence of only one Gaussian ATD (Figure 1B). Concerning the phenyl cation formation by fragmentation, it was assumed that the proton was initially located on the heteroatom (N-protonated aniline and O-protonated phenol), leading to the phenyl cation formation by direct bond dissociation (i.e., Aryl-NH_3^+ or Aryl-OH_2^+).

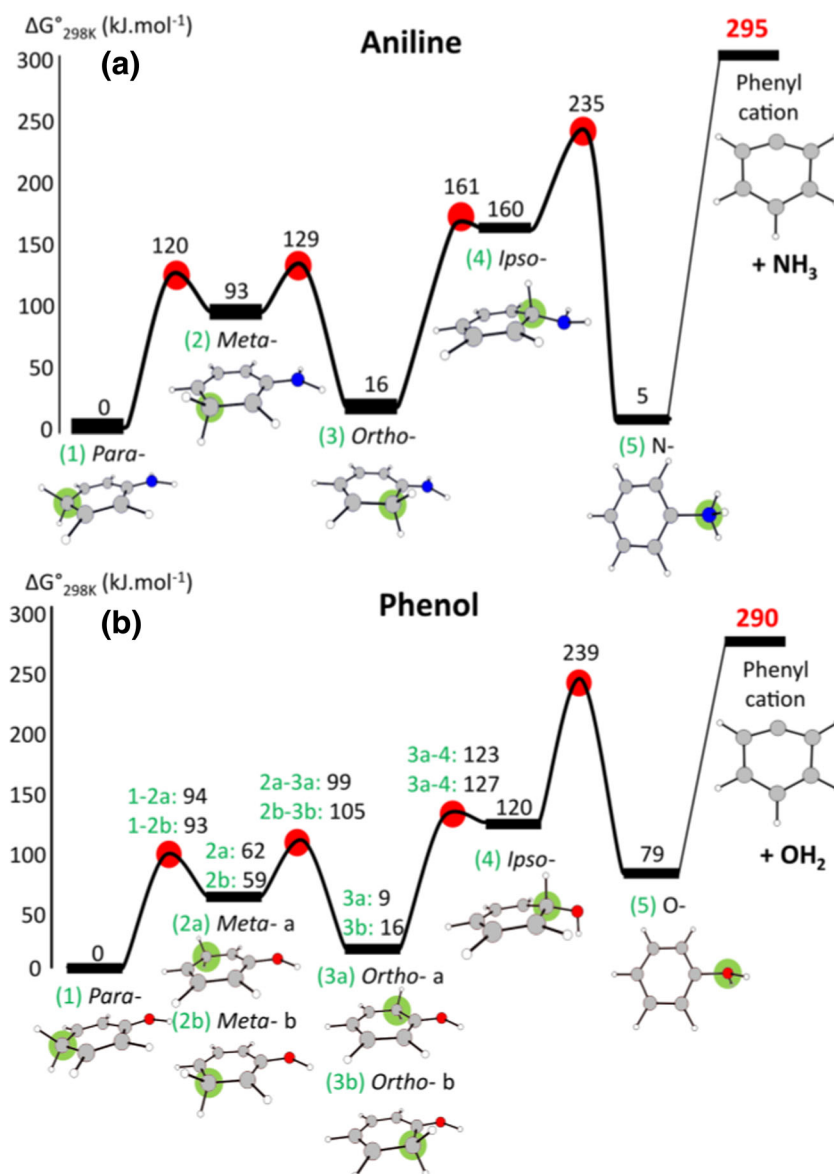


Figure 5. Reaction coordinate diagrams of protonated aniline tautomerization (a) and protonated phenol tautomerization (b). Relative Gibbs free energies (in kJ mol^{-1} , computed for 298.15 K and 1 atm using DFT with the cam-B3LYP pseudopotential and the 6-31++G(d,p) basis set) reported are relative to the most stable tautomers in each case (C_{para} -protonated aniline and C_{para} -protonated phenol). Stable and transition states are respectively represented with black lines and red spots. Stable structures are reported with green spots indicating the protonation site. Dissociation energy values to form a phenyl cation are indicated in red

The dissociation energies of Aryl-NH_3^+ (calculated by Eq. (1)) and Aryl-OH_2^+ (calculated by Eq. (2)) are 290 and 211 kJ mol^{-1} , respectively. A higher dissociation energy for Aryl-NH_3^+ than for Aryl-OH_2^+ is in perfect agreement with the experimental V_{50} values of protonated aniline and protonated phenol (see Figure 3). In both cases, the dissociation energies are still higher than the required activation energies for tautomerism, suggesting that proton transfers can occur before the dissociation energy is reached similarly to the mobile proton model of peptide fragmentation [41]. These proton transfers suggested by the theoretical calculations also support the detection of the phenyl cation as a fragment from C_{para} -protonated aniline. Indeed, C_{para} -protonated aniline can be converted to N-protonated aniline, which in turn fragments to form a phenyl cation with a subsequent neutral loss of ammonia (black double arrow in Scheme 2).

$$\Delta G_{\text{diss,C-N}}^0 = G_{\text{phenyl cation}}^0 + G_{\text{NH}_3}^0 - G_{\text{N-protonated aniline}}^0 \quad (1)$$

$$\Delta G_{\text{diss,C-O}}^0 = G_{\text{phenyl cation}}^0 + G_{\text{OH}_2}^0 - G_{\text{O-protonated phenol}}^0 \quad (2)$$

The reaction pathway of N-protonated aniline to O-protonated phenol conversion is reported in Figure 6. The tautomerization (black lines) and the two hypothetical mechanisms, $\text{S}_{\text{N}}1$ (blue line) and $\text{S}_{\text{N}}\text{Ar}$ (red line), were investigated. For the $\text{S}_{\text{N}}1$ mechanism, a blue trace is used to represent the phenyl cation as a stable intermediate of the nucleophilic substitution. For $\text{S}_{\text{N}}\text{Ar}$, a red trace is used to represent the activation energy barrier of the transition state. The reported energies in Figure 6 are Gibbs free energy variations (ΔG° in kJ mol^{-1}) relative to the C_{para} -protonated. The Gibbs free

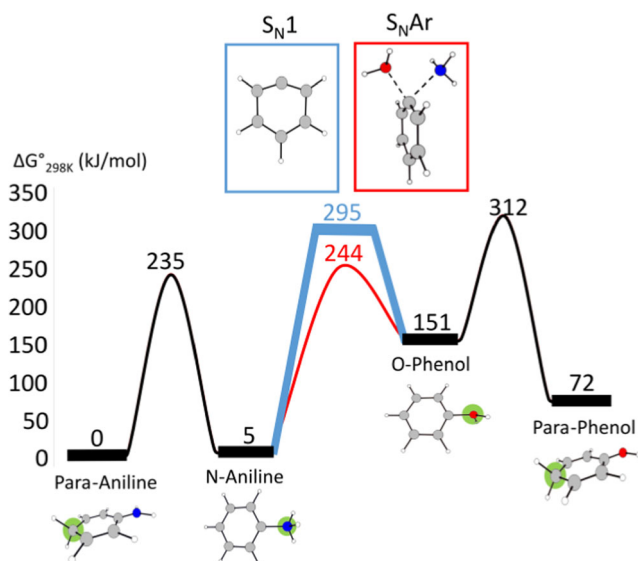


Figure 6. Reaction coordinate diagram of the protonated aniline to protonated phenol conversion. Relative Gibbs free energies are given in kJ mol^{-1} and computed for 298.15 K and 1 atm using DFT with the cam-B3LYP pseudopotential and the 6-31++G(d,p) basis set. $\text{S}_{\text{N}}1$ and $\text{S}_{\text{N}}\text{Ar}$ mechanisms are respectively reported in blue and red. Only the highest energy barriers obtained from Figure 5 for the tautomerization are reported

energy variation (ΔG°) values were again corrected to impose an identical element composition for all investigated states and compare their energies. In details, $\text{G}^\circ\text{H}_2\text{O}$ is added to the ΔG° of protonated aniline, the $\text{G}^\circ\text{NH}_3$ is added to the ΔG° of protonated phenol and both $\text{G}^\circ\text{H}_2\text{O}$ and $\text{G}^\circ\text{NH}_3$ are added to the ΔG° of phenyl cation. The reported energy barriers for tautomerization (in black line) correspond to the higher activation barrier calculated for the tautomerization process (Figure 5A, B). At first glance, these calculations suggest that the $\text{S}_{\text{N}}\text{Ar}$ mechanism is the preferential pathway for the formation of protonated phenol. However, since NH_3 is a better nucleophile than H_2O , the formation of N-protonated aniline from the transition state is favored. In the $\text{S}_{\text{N}}\text{Ar}$ mechanism, the formation of protonated phenol requires a large amount of water molecules. In this context, the $\text{S}_{\text{N}}1$ mechanism should occur in the TRAP, TRANSFER (CID cells), and IMS cells where only traces of water are available while the $\text{S}_{\text{N}}\text{Ar}$ should be favored in solution and possibly during the desolvation process (i.e., in the ion source). The attachment of a water molecule to N-protonated aniline, such as for the $\text{S}_{\text{N}}\text{Ar}$ mechanism, might also favor the tautomerization by assisting the proton transfer as suggested by Attygalle and coworkers for the tautomers of aminobenzoic acid [42].

Interestingly, Figure 6 shows that the N-protonated aniline substitution to O-protonated phenol (295 kJ mol^{-1}) is more favorable than the tautomerization of O-protonated phenol to C_{para} -protonated phenol (312 kJ mol^{-1}). This suggests that the population of O-protonated phenol would be kinetically trapped and barely converted to C_{para} -protonated phenol, which should experimentally lead to the presence of different distributions of protonated phenol tautomers. This assumption is in good agreement with the different experimentally observed ATDs provided in Figure 1B, C for the phenol and aniline infused during electrospray mass spectrometry experiments as pure aniline or pure phenol solution.

Theoretical CCS in CO_2 for the most stable aniline and phenol protomers were calculated with the trajectory method. Due to the lack of IMS calibrating substances in CO_2 , we compared the sequence of the migration times with those obtained from theoretical CCS. The ascending migration order of these protomers was C_{para} -protonated phenol (5.10 ms) = C_{para} -protonated phenol (5.15 ms) < O-protonated phenol (5.41 ms) < N-protonated aniline (6.01 ms). That was in good agreement with the theoretical CCS values computed in CO_2 , which were 119 \AA^2 for C_{para} -protonated phenol, 120 \AA^2 for C_{para} -protonated aniline, 124 \AA^2 for O-protonated aniline, and 128 \AA^2 for N-protonated aniline.

Conclusion

As suggested by our aniline and phenol IMMS results, the use of the CCS as a unique descriptor requires a thorough understanding of the gas-phase reactions that can occur during ion mobility experiments. The activation of the ions before or after the ion mobility cell allowed strong evidence of these gas-

phase reactions leading to the proposal of reaction mechanisms. In this context, the Synapt G1/G2 traveling wave ion mobility mass spectrometers are particularly well suited for this kind of experimental studies. IMMS has successfully been applied to investigate gas-phase reaction occurring on the protonated aniline and the protonated phenol such as tautomerization and nucleophilic substitution. The benefit of ATD peak width and peak shape data allowed the detection of various tautomers and their gas-phase reactions. Tandem mass spectrometry applied before and after the ion mobility separation was optimized to measure the different populations of aniline and phenol tautomer ions (precursors and product ions) as a function of the applied CID activation energy. The observed variations in these populations provided valuable information concerning the gas-phase reaction mechanism. The IMMS and tandem mass spectrometry data analysis allowed the determination of a reaction pathway of N-protonated aniline to O-protonated phenol by an S_N1 reaction with the phenyl cation as a reaction intermediate. This gas-phase conversion led to the detection of the O-protonated phenol (as a kinetically trapped species) while this tautomer was not observed by direct phenol infusion, probably due to the presence of high energy barriers. The reverse reaction (protonated phenol to protonated aniline) is also observed if ammonia is added in the IMMS drift gas and the phenyl cation is first formed by CID. Theoretical calculations were used to support the proposed reaction mechanisms. The involvement of phenol also completes the models proposed by Attygalle and coworkers, Begala, as well as Ranasinghe and Glish [19, 25, 39] including the prototropic tautomers and nucleophile addition (formally via S_N1 and S_NAr reactions) to the phenyl cation intermediate.

We also showed that the formation of protonated phenol from aniline depends on the water amount present in the drift gas. For this reason, we suggest the use of aniline infusion as a promising tool to estimate the amount of gas moisture. The experimental settings also potentially affect the ATD of target compounds. We therefore recommend the use of internal standard compounds such as aniline or other aromatic compounds to estimate the harshness of the IMMS settings. Nonetheless, a deeper investigation of the gas-phase reactions involving these internal standards as a function of the IMMS settings (e.g., moisture content, traveling wave settings, and ion activations) should be considered for this purpose.

References

- Causon, T.J., Hann, S.: Theoretical evaluation of peak capacity improvements by use of liquid chromatography combined with drift tube ion mobility-mass spectrometry. *J. Chromatogr. A*. **1416**, 47–56 (2015)
- Rainville, P.D., Wilson, I.D., Nicholson, J.K., Isaac, G., Mullin, L., Langridge, J.I., Plumb, R.S.: Ion mobility spectrometry combined with ultra performance liquid chromatography/mass spectrometry for metabolic phenotyping of urine: effects of column length, gradient duration and ion mobility spectrometry on metabolite detection. *Anal. Chim. Acta*. **982**, 1–8 (2017)
- Chalet, C., Hollebrands, B., Janssen, H.-G., Augustijns, P., Duchateau, G.: Identification of phase-II metabolites of flavonoids by liquid chromatography–ion-mobility spectrometry–mass spectrometry. *Anal. Bioanal. Chem.* **410**, 471–482 (2018)
- Gosciny, S., Joly, L., De Pauw, E., Hanot, V., Eppe, G.: Travelling-wave ion mobility time-of-flight mass spectrometry as an alternative strategy for screening of multi-class pesticides in fruits and vegetables. *J. Chromatogr. A*. **1405**, 85–93 (2015)
- Gosciny, S., McCullagh, M., Far, J., De Pauw, E., Eppe, G.: Towards the use of ion mobility mass spectrometry derived collision cross section as a screening approach for unambiguous identification of targeted pesticides in food. *Rapid Commun. Mass Spectrom.* **0**, (2019). <https://doi.org/10.1002/rcm.8395>
- Regueiro, J., Negreira, N., Berntssen, M.H.G.: Ion-mobility-derived collision cross section as an additional identification point for multiresidue screening of pesticides in fish feed. *Anal. Chem.* **88**, 11169–11177 (2016)
- Kune, C., Far, J., De Pauw, E.: Accurate drift time determination by traveling wave ion mobility spectrometry: the concept of the diffusion calibration. *Anal. Chem.* **88**, 11639–11646 (2016)
- Poyer, S., Comby-Zerbino, C., Choi, C.M., Macaleese, L., Deo, C., Bogliotti, N., Xie, J., Salpin, J.-Y., Dugourd, P., Chirof, F.: Conformational dynamics in ion mobility data. *Anal. Chem.* **89**, 4230–4237 (2017)
- Gabelica, V., Shvartsburg, A.A., Afonso, C., Barran, P., Benesch, J.L.P., Bleiholder, C., Bowers, M.T., Bilbao, A., Bush, M.F., Campbell, J.L., Campuzano, I.D.G., Causon, T., Clowers, B.H., Creaser, C.S., De Pauw, E., Far, J., Fernandez-Lima, F., Fjeldsted, J.C., Giles, K., Groessl, M., Hogan Jr., C.J., Hann, S., Kim, H.I., Kurulugama, R.T., May, J.C., McLean, J.A., Pagel, K., Richardson, K., Ridgeway, M.E., Rosu, F., Sobott, F., Thalassinou, K., Valentine, S.J., Wytenbach, T.: Recommendations for reporting ion mobility mass spectrometry measurements. *Mass Spectrom. Rev.* **0**, (2019). <https://doi.org/10.1002/mas.21585>
- Marchand, A., Livet, S., Rosu, F., Gabelica, V.: Drift tube ion mobility: how to reconstruct collision cross section distributions from arrival time distributions? *Anal. Chem.* **89**, 12674–12681 (2017)
- Muller, P.: Glossary of terms used in physical organic chemistry: (IUPAC Recommendations 1994). *Pure Appl. Chem.* **66**, 1077–1184 (1994)
- Chetverin, A.B.: Evidence for a diprotomeric structure of Na,K-ATPase. Accurate determination of protein concentration and quantitative end-group analysis. *FEBS Lett.* **196**, 121–125 (1986)
- Wood, K.V., Cooks, R.G., Burinsky, D.J., Cameron, D.: Site of gas-phase cation attachment. Protonation, methylation, and ethylation of aniline, phenol, and thiophenol. *J. Organomet. Chem.* **48**, 5236–5242 (1983)
- Karpas, Z., Berant, Z., Stimac, R.M.: An ion mobility spectrometry/mass spectrometry (IMS/MS) study of the site of protonation in anilines. *Struct. Chem.* **1**, 201–204 (1990)
- Smith, R.L., Chyall, L.J., Beasley, B.J., Kenttämaa, H.I.: The site of protonation of aniline. *J. Am. Chem. Soc.* **117**, 7971–7973 (1995)
- Russo, N., Toscano, M., Grand, A., Mineva, T.: Proton affinity and protonation sites of aniline. Energetic behavior and density functional reactivity indices. *J. Phys. Chem. A*. **104**, 4017–4021 (2000)
- Daniel Boese, A., Martin, J.M.L., De Proft, F., Geerlings, P.: The protonation site of aniline revisited: a “torture test” for electron correlation methods. *ACS Symp. Ser.* **958**, 183–192 (2007)
- Lalli, P.M., Iglesias, B.A., Toma, H.E., De Sa, G.F., Daroda, R.J., Silva Filho, J.C., Szulejko, J.E., Araki, K., Eberlin, M.N.: Protomers: formation, separation and characterization via travelling wave ion mobility mass spectrometry. *J. Mass Spectrom.* **47**, 712–719 (2012)
- Attygalle, A.B., Xia, H., Pavlov, J.: Influence of ionization source conditions on the gas-phase protomer distribution of anilinium and related cations. *J. Am. Soc. Mass Spectrom.* **28**, 1575–1586 (2017)
- Boschmans, J., Jacobs, S., Williams, J.P., Palmer, M., Richardson, K., Giles, K., Laphorn, C., Herrebout, W.A., Lemièrre, F., Sobott, F.: Combining density functional theory (DFT) and collision cross-section (CCS) calculations to analyze the gas-phase behaviour of small molecules and their protonation site isomers. *Analyst.* **141**, 4044–4054 (2016)
- Van Lau, K., Kebarle, P.: Substituent effects on the intrinsic basicity of benzene: proton affinities of substituted benzenes. *J. Am. Chem. Soc.* **98**, 7452–7453 (1976)
- DeFrees, D.J., McIver, R.T., Hehre, W.J.: The proton affinities of phenol. *J. Am. Chem. Soc.* **99**, 3853–3854 (1977)
- Tishchenko, O., Pham-Tran, N.-N., Kryachko, E.S., Nguyen, M.T.: Protonation of gaseous halogenated phenols and anisoles and its interpretation using DFT-based local reactivity indices. *J. Phys. Chem. A*. **105**, 8709–8717 (2001)

24. Campbell, J.L., Yang, A.M.-C., Melo, L.R., Hopkins, W.S.: Studying gas-phase interconversion of tautomers using differential mobility spectrometry. *J. Am. Soc. Mass Spectrom.* **27**, 1277–1284 (2016)
25. Ranasinghe, Y.A., Glish, G.L.: Reactions of the phenylium cation with small oxygen- and nitrogen-containing molecules. *J. Am. Soc. Mass Spectrom.* **7**, 473–481 (1996)
26. Giles, K., Pringle, S.D., Worthington, K.R., Little, D., Wildgoose, J.L., Bateman, R.H.: Applications of a travelling wave-based radio-frequency-only stacked ring ion guide. *Rapid Commun. Mass Spectrom.* **18**, 2401–2414 (2004)
27. Beegle, L.W., Kanik, I., Matz, L., Hill Jr., H.H.: Effects of drift-gas polarizability on glycine peptides in ion mobility spectrometry. *Int. J. Mass Spectrom.* **216**, 257–268 (2002)
28. Warnke, S., Seo, J., Boschmans, J., Sobott, F., Scrivens, J.H., Bleiholder, C., Bowers, M.T., Gewinner, S., Schöllkopf, W., Pagel, K., Von Helden, G.: Protomers of benzocaine: solvent and permittivity dependence. *J. Am. Chem. Soc.* **137**, 4236–4242 (2015)
29. Frisch, M., Trucks, G., Schlegel, H., Scuseria, G., Robb, M., Cheeseman, J., Scalmani, G., Barone, V., Mennucci, B., Petersson, G., Nakatsuji, H., Caricato, M., Li, X., Hratchian, H., Izmaylov, A., Bloino, J., Zheng, G., Sonnenberg, J., Hada, M., Ehara, M., Toyota, K., Fukuda, R., Hasegawa, J., Ishida, M., Nakajima, T., Honda, Y., Kitao, O., Nakai, H., Vreven, T., Montgomery, J., Peralta, J., Ogliaro, F., Bearpark, M., Heyd, J., Brothers, E., Kudin, K., Staroverov, V., Kobayashi, R., Normand, J., Raghavachari, K., Rendell, A., Burant, J., Iyengar, S., Tomasi, J., Cossi, M., Rega, N., Millam, J., Klene, M., Knox, J., Cross, J., Bakken, V., Adamo, C., Jaramillo, J., Gomperts, R., Stratmann, R., Yazyev, O., Austin, A., Cammi, R., Pomelli, C., Ochterski, J., Martin, R., Morokuma, K., Zakrzewski, V., Voth, G., Salvador, P., Dannenberg, J., Dapprich, S., Farkas, D.A., Foresman, J., Ortiz, J., Cioslowski, J., Fox, D.: Gaussian 09, Revision B.01. Gaussian 09 Revis. D01. Gaussian Inc, Wallingford (2009)
30. Peng, L., Hua, L., Wang, W., Zhou, Q., Li, H.: On-site rapid detection of trace non-volatile inorganic explosives by stand-alone ion mobility spectrometry via acid-enhanced evaporation. *Sci. Rep.* **4**, 6631 (2014)
31. Yanai, T., Tew, D., Handy, N.: A new hybrid exchange-correlation functional using the Coulomb-attenuating method (CAM-B3LYP). *Chem. Phys. Lett.* **393**, 51–57 (2004)
32. Larriba, C., Hogan, C.J.: Free molecular collision cross section calculation methods for nanoparticles and complex ions with energy accommodation. *J. Comput. Phys.* **251**, 344–336 (2013)
33. Larriba, C., Hogan, C.J.: Ion mobilities in diatomic gases: measurement versus prediction with non-specular scattering models. *J. Phys. Chem. A.* **117**, 3887–3901 (2013)
34. Shrivastav, V., Nahin, M., Hogan, C.J., Larriba-Andaluz, C.: Benchmark comparison for a multi-processing ion mobility calculator in the free molecular regime. *J. Am. Soc. Mass Spectrom.* **28**, 1540–1551 (2017)
35. Mesleh, M.F., Hunter, J.M., Shvartsburg, A.A., Schatz, G.C., Jarrold, M.F.: Structural information from ion mobility measurements: effects of the long-range potential. *J. Phys. Chem.* **100**, 16082–16086 (1996)
36. Wyttenbach, T., von Helden, G., Batka, J.J., Carlat, D., Bowers, M.T.: Effect of the long-range potential on ion mobility measurements. *J. Am. Soc. Mass Spectrom.* **8**, 275–282 (1997)
37. Wu, T., Derrick, J., Nahin, M., Chen, X., Larriba-Andaluz, C.: Optimization of long range potential interaction parameters in ion mobility spectrometry. *J. Chem. Phys.* **148**, 074102 (2018)
38. Kune, C., Haler, J.R.N., Far, J., De Pauw, E.: Effectiveness and limitations of computational chemistry and mass spectrometry in the rational design of target-specific shift reagents for ion mobility spectrometry. *ChemPhysChem.* **19**, 2921–2930 (2018)
39. Begala, M.: Conversion of benzoic acid into phenol in an ITMS under CI-MSn conditions. Recognition of ortho-chlorobenzoyl derivatives. *J. Mass Spectrom.* **53**, 30–38 (2018)
40. Purwaha, P., Silva, L.P., Hawke, D.H., Weinstein, J.N., Lorenzi, P.L.: An artifact in LC-MS/MS measurement of glutamine and glutamic acid: in-source cyclization to pyroglutamic acid. *Anal. Chem.* **86**, 5633–5637 (2014)
41. Paizs, B., Suhai, S.: Fragmentation pathways of protonated peptides. *Mass Spectrom. Rev.* **24**, 508–548 (2005)
42. Xia, H., Attygalle, A.B.: Transformation of the gas-phase favored O-protomer of p-aminobenzoic acid to its unfavored N-protomer by ion activation in the presence of water vapor: an ion-mobility mass spectrometry study. *J. Mass Spectrom.* **53**, 353–360 (2018)